Fully Printed and Flexible Schottky Diodes Based on Carbon Nanomaterials Operating Up to 5 MHz

Lorenzo Pimpolari, Irene Brunetti, Riccardo Sargeni, Francesco Pieri, Khaled Parvez, Massimo Macucci, *Member, IEEE*, Cinzia Casiraghi, and Gianluca Fiori, *Member, IEEE*

***Abstract*— The capability to fabricate printed and flexible energy harvesting and conditioning circuits, over a large area and with low-cost techniques, is crucial to enable flexible and wearable electronics. Carbon nanomaterials show excellent electrical, optical, chemical, and mechanical properties for printed electronics, offering low-cost, and large-area functionality on flexible substrates. In the past few years, many efforts have been dedicated to the fabrication of printed transistors made with carbon nanomaterials, but very few works have been dedicated to diodes, which are fundamental circuit elements, often employed in energy harvesting systems. Here we report a simple and cost-effective approach for the fabrication of fully inkjet-printed Schottky diodes on Kapton and paper substrates using carbon nanotubes (CNT) and graphene. We demonstrate that both ohmic and Schottky contacts between printed nanotubes and graphene can be obtained with post-printing thermal treatments at different temperatures. The diodes thus fabricated work with low supply voltages, exhibit excellent mechanical stability and have a maximum operating frequency in the order of 5 MHz.**

***Index Terms*— Carbon nanomaterials, carbon nanotubes (CNT), flexible diodes, flexible electronics, graphene, inkjet printed diodes, paper electronics.**

I. Introduction

A PRECONDITION for the success of portable, wearable, and flexible electronics is the capability of designing and fabricating circuits to supply and condition power [1], [2]. There are many situations, including, for example, radio frequency identifiers (RFID), near field communication tags, or sensors, in which power is supplied with an electromagnetic wave or is scavenged from the environmental electromagnetic field [3], [4]. In such situations, which are recurrent within the Internet of Things paradigm, diodes represent fundamental circuit elements, and they need to efficiently operate at low voltages at least in the high frequency (HF, 3–30 MHz) band, but also up to the ultra HF (UHF, 300–3000 MHz) band [3], [5], [6]. In particular, Schottky diodes are usually preferred for these applications because, as unipolar devices, they generally have shorter switching times (and can then work at HFs) and exhibit a lower voltage drop (which is particularly relevant in the case of energy scavenging) as compared, for example, to p-n junction diodes [7]. The challenge is then to find suitable materials (both semiconductors and metals) for the fabrication on flexible substrates and large-scale production.

Solution-processable materials are probably the most promising candidates, as they can be cost-effectively deposited over a large area using high-throughput techniques compatible with direct printing on different flexible substrates [8], [9], [10]. Numerous diodes based on solution processed low-dimensional [11], [12], [13], [14], organic [15], [16], [17], [18], [19], [20], [21], and metal-oxide [22], [23], [24], [25] semiconductors have been reported on both rigid and flexible substrates. Among the various available solution-processable materials, carbon-based nanomaterials, such as semiconducting carbon nanotubes (CNT) and graphene, have demonstrated compatibility with printing techniques and remarkable properties in printed devices [26], [27], [28]. Printed networks of semiconducting CNT are particularly promising for the future mass development of high-speed flexible electronics, since they have already demonstrated great potential when used as transistor channels [29], [30], achieving operating frequencies in the UHF range [31], as well as an intrinsic frequency of over 18 GHz for transistors with micrometric channel length [32]. However, to date, most research has been focusing on transistors, and no two-terminal diodes based on printed CNT have yet been reported.

In this article, we demonstrate a simple and effective method to fabricate low-cost, fully inkjet printed diodes on flexible substrate using graphene and single-walled CNT as contacts and p-type semiconductor, respectively. Device asymmetry is achieved by thermal annealing at different temperatures, which can be adjusted to obtain both an ohmic and a Schottky graphene–CNT contact. Devices fabricated on polyimide (Kapton) show good electrical properties, with an operating frequency of up to 5 MHz and excellent mechanical stability. Furthermore, we demonstrate the possibility of extending the proposed method to fabricate diodes on paper, which is an ideal substrate to enable sustainable flexible electronics due to its low cost, recyclability and biodegradability [33], [34].

II. Materials and Methods

Kapton (from DuPont) and paper (PEL P60, from Printed Electronics Ltd.) were used as substrates. Commercial silver and PEDOT:PSS inks (nanoparticle silver ink, from Sigma-Aldrich and Clevios PH 1000, from Heraeus) were used to

Manuscript received 15 September 2022; accepted 4 October 2022. Date of publication 21 October 2022; date of current version 10 November 2022. This work was supported in part by Printable Electronics on Paper through 2D materials based inks (ERC PEP2D) under Contract 770047, in part by Wearable Applications enabled by electronic Systems on Paper (H2020 WASP) under Contract 50 825213, and in part by the Graphene Flagship Core3 under Contract 881603. *(Corresponding author: Lorenzo Pimpolari.)*

Lorenzo Pimpolari was with the Dipartimento di Ingegneria dell'Informazione, University of Pisa, 56122 Pisa, Italy. He is now with the Instituto de Microelectrónica de Barcelona, IMB-CNM (CSIC), Cerdanyola del Vallès, 08193 Barcelona, Spain (e-mail: lorenzo.pimpolari@ing.unipi.it).

Irene Brunetti was with the Dipartimento di Ingegneria dell'Informazione, University of Pisa, 56122 Pisa, Italy. She is now with the InnovationLab, 69115 Heidelberg, Germany.

Riccardo Sargeni, Francesco Pieri, Massimo Macucci, and Gianluca Fiori are with the Dipartimento di Ingegneria dell'Informazione, University of Pisa, 56122 Pisa, Italy.

Khaled Parvez and Cinzia Casiraghi are with the Department of Chemistry, University of Manchester, M139PL Manchester, U.K.

This article has supplementary downloadable material available at https://doi.org/10.1109/JFLEX.2022.3215928, provided by the authors.

Digital Object Identifier 10.1109/JFLEX.2022.3215928

print the metal contacts. The graphene contacts were instead printed starting from custom-made aqueous ink with a concentration of ∼2 mg · mL^{-1}, whose preparation details have been reported elsewhere [35]. A commercial 99.9% semiconducting single-walled CNT toluene solution (IsoSol-S100, from NanoIntegris) with a concentration of 0.2 mg · mL^{-1} in toluene and average diameter and length of the CNT of 1.4 nm and 1 μm, respectively, was used as semiconductor. A characterization of the inkjet printed network from this formulation is available in previous work by our group [36].

Prior to printing, Kapton was washed in deionized water and dried with nitrogen. All materials were deposited by inkjet printing using a Fujifilm Dimatix Materials Printer 2850, equipped with 10 pL cartridges. CNT on Kapton and paper were printed with a drop spacing of 20 μm and a single print pass. Graphene and PEDOT:PSS were printed on Kapton with a drop spacing of 30 μm and 20 print passes, while silver with a single pass and drop spacing of 40 μm. Each thermal treatment was carried out on a hot plate in air for 20 min. All the electrical measurements were performed under ambient conditions. The current–voltage (I–V) characteristics were measured with a Keithley 4200A semiconductor characterization system. For the dynamic measurements, a function generator Siglent SDG2122X was used, with a value of the load resistor and capacitor of 100 MΩ and 1 nF, respectively. These values were chosen to be much higher than the series resistance and capacitance of the device in order not to alter the measurement.

III. Results and Discussion

A. Inkjet Printed Devices With Different Metal Pairs

The devices have been inkjet printed on Kapton using the CNT network as the semiconductor, and considering different combinations of metals for the contacts. Kapton has been selected as the main substrate because of its low roughness, relatively high glass-transition temperature and high bendability [37], while inkjet printing has been chosen as the fabrication technique because it is a cost-effective, mask-less process which allows deposition of materials under ambient conditions, with good control over deposited volume and lateral resolution [38]. The main advantages of the proposed approach lie in its simplicity, low cost, and compatibility with flexible substrates, which are among the key requirements for printable and flexible electronics [5], [39]. Fig. 1(a) shows a schematic cross section of the devices, with metals 1 and 2 indicating the different materials used for the contacts, i.e., silver, graphene and poly(3,4-ethylenedioxythiophene) polystyrene sulfonate (PEDOT:PSS). Fig. 1(b)–(d) shows the measured I–V characteristics for devices with different metal pairs, i.e., silver and graphene [Fig. 1(b)], PEDOT:PSS and graphene [Fig. 1(c)], silver and PEDOT:PSS [Fig. 1(d)].

For an ideal p-type semiconductor–metal interface, the Schottky barrier height (SBH, ϕ_B) is predicted based on the alignment of energy levels by the Schottky–Mott rule [40]

$$\phi_B = I_p - \phi_M \tag{1}$$

where I_p is the ionization energy of the semiconductor (given by the sum of its electronic affinity and bandgap energy) and ϕ_M the work function of the metal. Despite the different work functions of the metals [41], [42], [43], [44], [45], which should lead to different SBHs, our results show that all the I–V characteristics are symmetric, regardless of metal configuration. The complete symmetry of the measured I–V

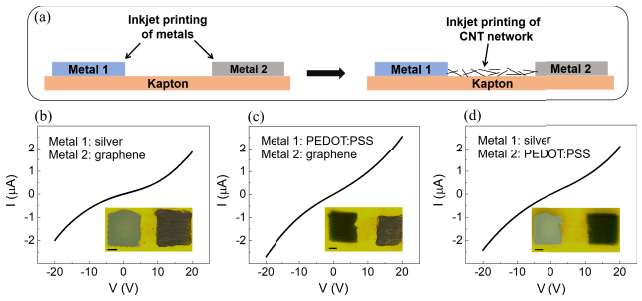

Fig. 1. (a) Schematic showing the fabrication sequence. I–V characteristics of devices with different combinations of contacts: (b) silver and graphene, (c) PEDOT:PSS and graphene, and (d) silver and PEDOT:PSS. Corresponding optical micrographs (scale bars are 75 μm) (insets).

suggests that SBHs are virtually independent of metals. This may be ascribed to the pinning of the Fermi level, which could originate from the formation of surface states in the semiconductor bandgap at the junction with the metal [46]. If the interface state density is high, the Fermi level of the metal is pinned at a level within the semiconductor bandgap, which depends on the energy level of the interface states, ϕ_I. In this case, (1) can be modified as follows [47]:

$$\phi_B = (I_p - \phi_I) - S(\phi_M - \phi_I) \tag{2}$$

where $S = |\partial\phi_B/\partial\phi_M|$ is the pinning factor: if $S = 1$, there is an unpinned interface (Schottky limit), and (2) reduces to (1); if $S = 0$, there is maximum pinning of the Fermi level (Bardeen limit), and (2) becomes independent of the electrical properties of the metal. Our results suggest that the pinning is close to the Bardeen limit, in accordance with previous literature, where small S values (<0.1) have often been reported for interfaces with low-dimensional materials [48], [49], [50], [51]. This explains why SBHs values are rarely in agreement with the experimental results obtained from devices made with both conventional and low-dimensional materials [50], [52], [53], [54].

B. Effect of the Annealing Temperature

Fig. 2(a) and (b) shows the changes in the I–V characteristic of a device with graphene used for both contacts, obtained using different annealing temperature T_A (from 50 °C to 275 °C). For these measurements, the device was initially cured at the lowest T_A and subsequently measured at room temperature. Then it was cured at a higher T_A and re-measured at room temperature, and so on. As expected, the behavior of the printed CNT–graphene contact significantly differs from that of a single nanotube-graphene contact investigate theoretically [55]. Thermal treatment leads to a change in the device resistance, which decreases as T_A increases. This is likely due to the evaporation of the solvent (toluene, which has a low boiling point and therefore partially evaporates even at low T_A) and to binder degradation promoted by the thermal annealing, resulting in an improved carrier transport across CNT–CNT and CNT–graphene junctions [56], [57], [58]. As can be observed, T_A has a significant influence on the nature of the contact between printed graphene and the CNT network, turning from the Schottky barrier into ohmic for T_A above 200 °C.

To further investigate this effect, we have carried out four-probe measurements. The dependence of both the semiconductor sheet resistance and the specific contact resistance of the printed graphene–CNT as a function of T_A is reported in

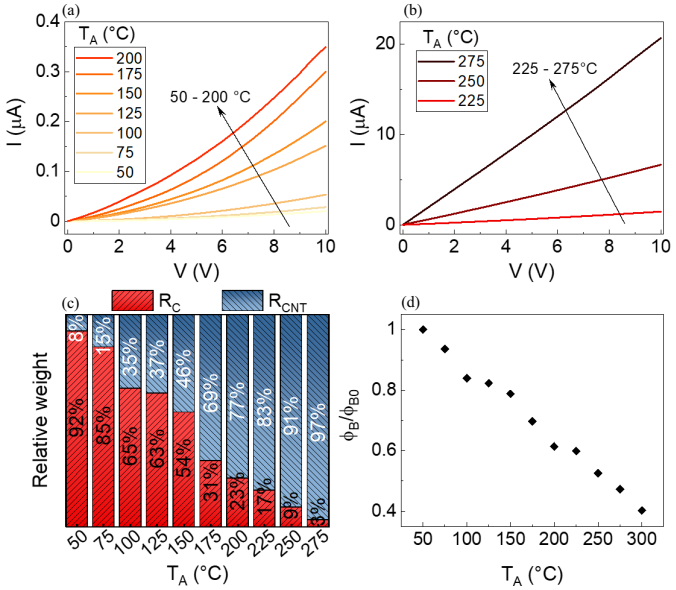

Fig. 2. I–V characteristics for different T_A (a) from 50 °C to 200 °C and (b) from 225 °C to 275 °C. (c) Relative weight of R_{CNT} and R_C on the total device resistance for different T_A. (d) Normalized SBH as a function of T_A.

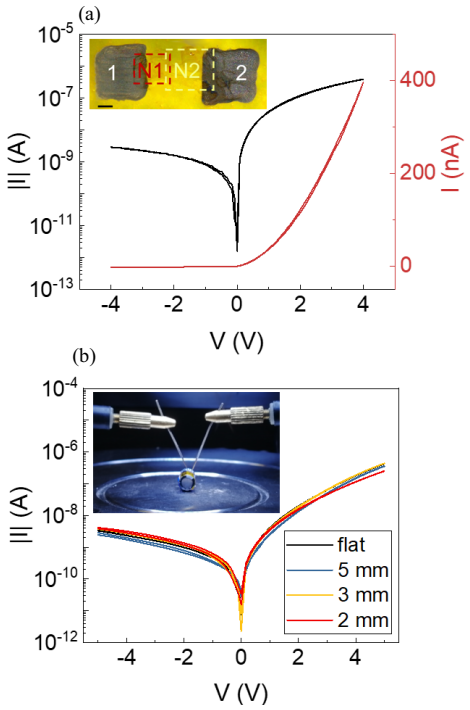

Fig. 3. (a) I–V characteristic of a printed diode both in semilogarithmic (left axis, black curve) and linear (right axis, red curve) scale. Optical micrograph of a device (scale bar is 100 μm) (inset). (b) I–V characteristics of a device for different bending radii, down to 2 mm. Photograph of the devices under bending (inset).

Fig. S1. Both quantities decrease significantly with T_A, and the reduction is more pronounced for the contact resistance (about four orders of magnitude). The total resistance of the device is given by the contribution of the semiconductor resistance, R_{CNT}, and the contact resistance, R_C (the graphene resistance can be neglected, as shown in Fig. S2). Fig. 2(c) shows the relative weight of R_C and R_{CNT} over the total resistance for a one-square device (i.e., a device in which the length L and width W of the semiconductor are the same) for different T_A. As can be observed, R_c is the major contributor on the total resistance for low T_A, while it becomes negligible as a result of annealing at relatively high temperatures (>200 °C).

The SBH in the case of thermionic emission can be expressed by the following formula [50]:

$$\phi_B = \frac{kT}{q}\ln\left(\frac{A_C A^* T^2}{I_S}\right) \tag{3}$$

where k is the Boltzmann's constant, T the temperature, q the elementary electric charge, A_C the contact area, A^* the Richardson constant, and I_s the reverse saturation current (which can be extracted as the y-axis intercept of the $\ln(I)$ versus V plot). An accurate evaluation of SBH is not possible, due to the uncertainty of the value of A^* for a network of printed CNT. Regardless of the actual value of ϕ_B, however, is it possible to evaluate its relative variation as a function of the annealing temperature. Fig. 2(d) shows the normalized SBH (ϕ_B/ϕ_{B0}, where ϕ_{B0} is the SBH for $T_A = 50$ °C) as a function of T_A. Consistently with what has been observed for the contact resistance, we notice a significant reduction of the SBH as T_A increases.

C. Inkjet Printed Diodes on Kapton

We exploit the dependence of the SBH on the annealing temperature to demonstrate in-plane, fully inkjet-printed rectifying devices by combining networks of CNT and graphene contacts treated at different annealing conditions. The fabrication starts by printing one graphene contact on Kapton (labeled as contact 1) and a printed CNT network (N1), as shown in the inset of Fig. 3(a). A thermal treatment at 250 °C follows, which makes the printed graphene–CNT contact ohmic, as previously demonstrated. The second graphene contact (contact 2) is then printed together with the second region of the CNT network (N2), which slightly overlaps region N1 [inset of Fig. 3(a)]. The fabrication process ends with a thermal treatment at 150 °C. This annealing temperature results in a good compromise, as it allows to get a barrier high enough to obtain an acceptable rectification ratio while reducing the series resistance introduced by N2. The latter is a crucial aspect as N2 is the part of the device that introduces the highest series resistance (along with the relative contact resistance): its reduction is therefore fundamental in order to reduce the total series resistance of the diode, R_s. For the same reason, it is also important to shorten the length of N2 (L_2) or to enlarge its width (W_2). The interface between the N1 and N2 regions is ohmic, as shown in Fig. S3.

The I–V characteristic of a device fabricated following the described procedure is reported in Fig. 3(a), both in semilogarithmic and the linear scale. The device is biased between contact 1 (anode) and contact 2 (cathode) and has an overall network width and length of 250 and 150 μm, respectively. A clear rectifying behavior can be observed, with a rectification factor (defined as the ratio between the forward current evaluated at a certain voltage $V_X > 0$ and the reverse current evaluated at $-V_x$) of $\sim 10^2$ at 4 V. The polarity is consistent with that expected in the case of a p-type semiconductor–metal junction. A fitting of a diode characteristic using the Shockley equation is reported in Fig. S4.

The height profile of a CNT network printed on SiO_2 is shown in Fig. S5. The average thickness t is about 25 nm, in line with those reported in the literature for printed networks [59], [60]. Considering this thickness, the forward

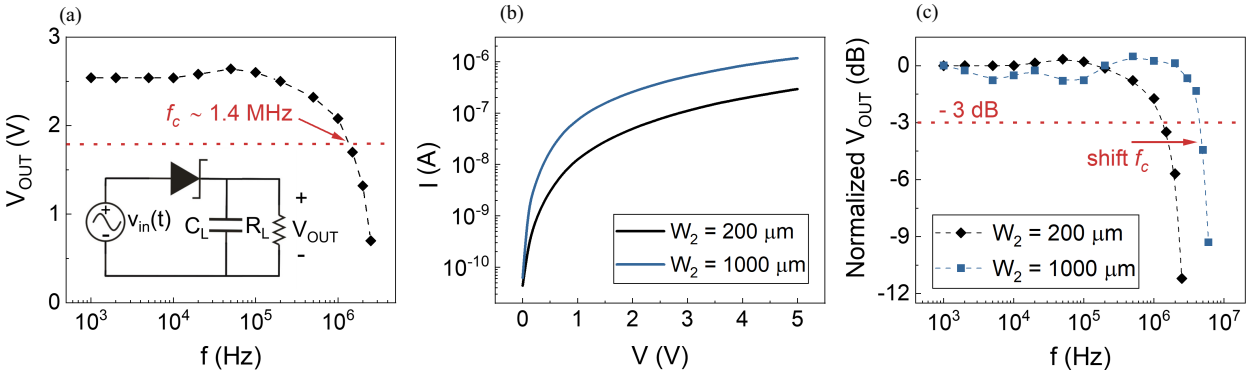

Fig. 4. (a) Measured V_{OUT} as a function of f (V_{IN} = 4 V). The dotted line represents the voltage level corresponding to a reduction of 3 dB from the maximum V_{OUT}. Schematic of the half-wave rectifier (inset). (b) Forward I–V characteristics and (c) Bode plot of V_{OUT} for two devices with different W_2.

current density [$J = I/(Wt)$] for the device whose I–V characteristic is shown in Fig. 3(a) is of the order of 5 A · cm^2 at 4 V (see Fig. S6). In Fig. S7 the J–V characteristics of four different devices are reported.

The printed diodes exhibit negligible hysteresis and can operate with moderate supply voltages (of the order of a few volts). In addition, the adopted method allows using the same metal for both contacts, while leveraging printed graphene, which is a low-cost material, with good electric conductivity and excellent mechanical properties [61], [62], [63]. Also considering the high flexibility reported for CNT networks [64], these devices are particularly promising for flexible applications. To confirm this, we have carried out bending measurements of the printed diodes on Kapton. Tensile stress is applied to the devices by wrapping the substrate on cylindrical supports with different radii (r): 5, 3, and 2 mm. The I–V characteristic measured under different bending conditions are reported in Fig. 3(b). There are no major changes under the different bending conditions, although for the smaller investigated value r = 2 mm, there is a slight reduction in the forward current and an increase in the reverse current. The effect, however, is reversible since the characteristic returns to its original values once the strain is removed, demonstrating very good stability of the diodes against mechanical bending.

D. Dynamic Response

One of the most important figures of merit for determining the performance of a diode is its maximum operating frequency [3], [5]. Different figures of merit exist to define the maximum operating frequency of a Schottky diode. Among them, one of the most frequently used is the 3-dB cutoff frequency, f_c, which is usually extracted by inserting the diode in the half-rectifying configuration shown in the inset of Fig. 4(a) [21], [65]. The input generator provides a single harmonic signal v_{in} at frequency f and amplitude V_{IN} [$v_{in}(t) = V_{IN}$ sin($2\pi ft$)]. R_L and C_L are the load resistor and capacitor, respectively, and are chosen to be much higher than those of the diode, in order not to affect its frequency response. f_c is the frequency at which the output voltage (V_{OUT}, measured with a multimeter) is attenuated by 3 dB with respect to the maximum V_{OUT} (that is, V_{OUT} extracted for low frequencies). Fig. 4(a) shows the measured V_{OUT} for a diode printed on Kapton as a function of the frequency of the input signal. The 3-dB cutoff frequency is found to be ~1.4 MHz.

It is further possible to increase the operating frequency range by adjusting the device dimensions. The cutoff frequency is, indeed, inversely proportional to the diode series resistance [65]. As mentioned, R_s is primarily limited by the printed region N2 and the relative contact. It is therefore possible to reduce R_s by modifying the geometry of N2. Fig. 4(b) shows the I–V characteristics in the forward region for two devices with the same L_2 but different W_2 (200 and 1000 μm). As expected, the device with higher W_2 exhibits lower R_s. This reflects in an increase of the 3-dB cutoff frequency, as shown in the Bode Fig. 4(c). f_c reaches a value close to 5 MHz for the wider device, which is within the HF range. This value is in line with or better than several organic and inorganic solution-processed diodes [15], [16], [20], [66], although not comparable to the best results in literature [18], [25], [67]. With further optimizations, the cutoff frequency can be increased, for example, with the goal of achieving 13.56 MHz, a frequency widely used for RFID tags [68].

E. Inkjet Printed Diodes on Paper

Finally, we show that the proposed method can also be used for the fabrication of printed diodes on paper, which is a porous substrate with a higher surface roughness compared to plastic substrates. Moreover, the relatively high annealing temperatures used to cure the devices on Kapton are not compatible with a thermally sensitive substrate such as paper (the employed paper can withstand a maximum temperature of about 120 °C). However, it is necessary to take into account that the properties of paper are rather different from those of a plastic substrate such as Kapton. This is reflected in a different electrical conduction between devices printed on paper and on Kapton. Fig. 5(a) and (b) show, respectively, the effect of T_A on the I–V characteristics and total resistance (R_T) for a one-square device on paper (formed by a unique CNT network). As can be observed from the comparison with Fig. 2, currents are higher (and resistances lower) for devices on paper with the same dimensions. This may be due to the fact that paper absorbs some of the solvent from the ink, which therefore has less impact on conduction at low annealing temperatures.

Fig. 5(c) shows the I–V characteristic of a diode obtained with the same previously described procedure, but with a single heat treatment at 120 °C after printing contact 1 and N1, while contact 2 and N2 are untreated. It can be noticed that the diode on paper exhibits a significantly larger hysteresis than those on Kapton. This might be due to the presence of traps at the interface between the CNT network and the rough paper substrate, as well as to the reduced annealing temperature. Other post-processing treatments could be beneficial and allow to treat the device in a way compatible with the substrate.

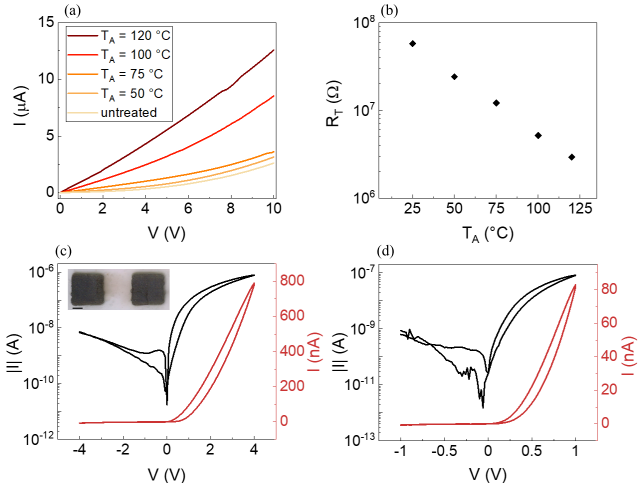

Fig. 5. (a) I–V characteristics for a device on paper, from untreated to cured at 120 °C. (b) Total resistance as a function of T_A for a device with $L = W$. I–V characteristics of the same diode printed on paper, both in semilogarithmic (left axis, black curve) and linear (right axis, red curve) scale, in the voltage range (c) ±4 and (d) ±1 V. The diode has an overall network width and length of 250 and 300 μm, respectively. Optical micrograph of a diode on paper (scale bar is 100 μm) [inset in (c)].

For example, fast laser and photonic annealing have been successfully employed to cure printed materials on low glass-transition temperature substrates [62], [69]. However, even in this case the device exhibits good electrical properties with a rectifying factor $>10^2$ at 4 V. In addition, diodes on paper have a rectification factor in the order of 10^2 even in the ±1 V voltage range [see Fig. 5(d)], and are therefore suitable for operating at very low voltages. The I–V characteristics of four different diodes in the ±1 V range are shown in Fig. S9. We have also carried out bending measurements for the diode on paper, reported in Fig. S10, which show good stability of the characteristics down to bending radii of 5 mm.

IV. Conclusion

We have demonstrated a simple, low-cost approach that exploits the dependence of the SBH on the annealing temperature to demonstrate in-plane, fully inkjet-printed rectifying devices by combining networks of CNT and graphene contacts treated at different temperatures. The devices printed on Kapton have shown a rectification ratio up to 10^2, operating at voltages of a few volts, stability against substrate bending down to 2 mm, and maximum operating frequency in the order of 5 MHz. We have also demonstrated diodes on paper fabricated with the same method that can operate with a voltage of the order of 1 V.

Present results are relevant for the development of a broad range of applications that require flexible, printed, and low-cost diodes.

References

[1] A. M. Zamarayeva et al., "Flexible and stretchable power sources for wearable electronics," *Sci. Adv.*, vol. 3, no. 6, Jun. 2017, Art. no. e1602051, doi: 10.1126/sciadv.1602051.

[2] P. Wang et al., "The evolution of flexible electronics: From nature, beyond nature, and to nature," *Adv. Sci.*, vol. 7, no. 20, Oct. 2020, Art. no. 2001116, doi: 10.1002/advs.202001116.

[3] J. Semple, D. G. Georgiadou, G. Wyatt-Moon, G. Gelinck, and T. D. Anthopoulos, "Flexible diodes for radio frequency (RF) electronics: A materials perspective," *Semicond. Sci. Technol.*, vol. 32, no. 12, Oct. 2017, Art. no. 123002, doi: 10.1088/1361-6641/aa89ce.

[4] V. Surducan, E. Surducan, and R. Gutt, "Harvesting and conversion of the environmental electromagnetic pollution into electrical energy by novel rectenna array coupled with resonant micro-converter," *Energy*, vol. 211, Nov. 2020, Art. no. 118645, doi: 10.1016/j.energy.2020.118645.

[5] Y. Chu, C. Qian, P. Chahal, and C. Cao, "Printed diodes: Materials processing, fabrication, and applications," *Adv. Sci.*, vol. 6, no. 6, Mar. 2019, Art. no. 1801653, doi: 10.1002/advs.201801653.

[6] X. Zhang et al., "Two-dimensional MoS_2-enabled flexible rectenna for Wi-Fi-band wireless energy harvesting," *Nature*, vol. 566, no. 7744, pp. 368–372, Feb. 2019, doi: 10.1038/s41586-019-0892-1.

[7] A. Di Bartolomeo, "Graphene Schottky diodes: An experimental review of the rectifying graphene/semiconductor heterojunction," *Phys. Rep.*, vol. 606, pp. 1–58, Jan. 2016, doi: https://doi.org/10.1016/j.physrep.2015.10.003.

[8] D. B. Mitzi, "Solution-processed inorganic semiconductors," *J. Mater. Chem.*, vol. 14, no. 15, p. 2355, 2004, doi: 10.1039/b403482a.

[9] S. Allard, M. Forster, B. Souharce, H. Thiem, and U. Scherf, "Organic semiconductors for solution-processable field-effect transistors (OFETs)," *Angew. Chem. Int. Ed.*, vol. 47, no. 22, pp. 4070–4098, May 2008, doi: 10.1002/anie.200701920.

[10] F. Bonaccorso, A. Bartolotta, J. N. Coleman, and C. Backes, "2D-crystal-based functional inks," *Adv. Mater.*, vol. 28, no. 29, pp. 6136–6166, Aug. 2016, doi: 10.1002/adma.201506410.

[11] C. Biswas, S. Y. Lee, T. H. Ly, A. Ghosh, Q. N. Dang, and Y. H. Lee, "Chemically doped random network carbon nanotube p-n junction diode for rectifier," *ACS Nano*, vol. 5, no. 12, pp. 9817–9823, 2011, doi: 10.1021/nn203391h.

[12] A. Kaur, X. Yang, K. Y. Park, and P. Chahal, "Reduced graphene oxide based Schottky diode on flex substrate for microwave circuit applications," in *Proc. IEEE 63rd Electron. Compon. Technol. Conf.*, May 2013, pp. 1037–1042, doi: 10.1109/ECTC.2013.6575700.

[13] A. Kaur, X. Yang, and P. Chahal, "CNTs and graphene-based diodes for microwave and millimeter-wave circuits on flexible substrates," *IEEE Trans. Compon., Packag., Manuf. Technol.*, vol. 6, no. 12, pp. 1766–1775, Dec. 2016, doi: 10.1109/TCPMT.2016.2586023.

[14] C. Chen et al., "Carbon nanotube intramolecular p-i-n junction diodes with symmetric and asymmetric contacts," *Sci. Rep.*, vol. 6, no. 1, p. 22203, Apr. 2016, doi: 10.1038/srep22203.

[15] K. E. Lilja, T. G. Bäcklund, D. Lupo, T. Hassinen, and T. Joutsenoja, "Gravure printed organic rectifying diodes operating at high frequencies," *Organic Electron.*, vol. 10, no. 5, pp. 1011–1014, Aug. 2009, doi: 10.1016/j.orgel.2009.04.008.

[16] W.-W. Tsai, Y.-C. Chao, E.-C. Chen, H.-W. Zan, H.-F. Meng, and C.-S. Hsu, "Increasing organic vertical carrier mobility for the application of high speed bilayered organic photodetector," *Appl. Phys. Lett.*, vol. 95, no. 21, Nov. 2009, Art. no. 213308, doi: 10.1063/1.3263144.

[17] S. Altazin et al., "Physics of the frequency response of rectifying organic Schottky diodes," *J. Appl. Phys.*, vol. 115, no. 6, Feb. 2014, Art. no. 064509, doi: 10.1063/1.4865739.

[18] C.-M. Kang et al., "1 GHz pentacene diode rectifiers enabled by controlled film deposition on SAM-treated Au anodes," *Adv. Electron. Mater.*, vol. 2, no. 2, Feb. 2016, Art. no. 1500282, doi: 10.1002/aelm.201500282.

[19] S. G. Higgins, T. Agostinelli, S. Markham, R. Whiteman, and H. Sirringhaus, "Organic diode rectifiers based on a high-performance conjugated polymer for a near-field energy-harvesting circuit," *Adv. Mater.*, vol. 29, no. 46, Dec. 2017, Art. no. 1703782, doi: 10.1002/adma.201703782.

[20] M. Cao, W. J. Hyun, L. F. Francis, and C. D. Frisbie, "Inkjet-printed, self-aligned organic Schottky diodes on imprinted plastic substrates," *Flexible Printed Electron.*, vol. 5, no. 1, Jan. 2020, Art. no. 015006, doi: 10.1088/2058-8585/ab670a.

[21] F. A. Viola et al., "A 13.56 MHz rectifier based on fully inkjet printed organic diodes," *Adv. Mater.*, vol. 32, no. 33, Aug. 2020, Art. no. 2002329, doi: 10.1002/adma.202002329.

[22] H. Park, H. Kang, Y. Lee, Y. Park, J. Noh, and G. Cho, "Fully roll-to-roll gravure printed rectenna on plastic foils for wireless power transmission at 13.56 MHz," *Nanotechnology*, vol. 23, no. 34, Aug. 2012, Art. no. 344006, doi: 10.1088/0957-4484/23/34/344006.

[23] J. Semple et al., "Radio frequency coplanar ZnO Schottky nanodiodes processed from solution on plastic substrates," *Small*, vol. 12, no. 15, pp. 1993–2000, Apr. 2016, doi: 10.1002/smll.201503110.

[24] M. Li et al., "0.7-GHz solution-processed indium oxide rectifying diodes," *IEEE Trans. Electron Devices*, vol. 67, no. 1, pp. 360–364, Jan. 2020, doi: 10.1109/TED.2019.2954167.

[25] D. G. Georgiadou et al., "100 GHz zinc oxide Schottky diodes processed from solution on a wafer scale," *Nature Electron.*, vol. 3, no. 11, pp. 718–725, Nov. 2020, doi: 10.1038/s41928-020-00484-7.
[26] E. B. Secor and M. C. Hersam, "Emerging carbon and post-carbon nanomaterial inks for printed electronics," *J. Phys. Chem. Lett.*, vol. 6, no. 4, pp. 620–626, 2015, doi: 10.1021/jz502431r.
[27] K. Chen et al., "Printed carbon nanotube electronics and sensor systems," *Adv. Mater.*, vol. 28, pp. 4397–4414, Jun. 2016, doi: 10.1002/adma.201504958.
[28] F. Torrisi and T. Carey, "Graphene, related two-dimensional crystals and hybrid systems for printed and wearable electronics," *Nano Today*, vol. 23, pp. 73–96, Dec. 2018, doi: 10.1016/j.nantod.2018.10.009.
[29] M. Ha et al., "Printed, sub-3V digital circuits on plastic from aqueous carbon nanotube inks," *ACS Nano*, vol. 4, no. 8, pp. 4388–4395, Aug. 2010, doi: 10.1021/nn100966s.
[30] S. Lu et al., "Flexible, print-in-place 1D–2D thin-film transistors using aerosol jet printing," *ACS Nano*, vol. 13, no. 10, pp. 11263–11272, Oct. 2019, doi: 10.1021/acsnano.9b04337.
[31] J. Vaillancourt et al., "All ink-jet-printed carbon nanotube thin-film transistor on a polyimide substrate with an ultrahigh operating frequency of over 5 GHz," *Appl. Phys. Lett.*, vol. 93, no. 24, Dec. 2008, Art. no. 243301, doi: 10.1063/1.3043682.
[32] P. M. Grubb, H. Subbaraman, S. Park, D. Akinwande, and R. T. Chen, "Inkjet printing of high performance transistors with micron order chemically set gaps," *Sci. Rep.*, vol. 7, no. 1, p. 1202, Dec. 2017, doi: 10.1038/s41598-017-01391-2.
[33] D. Tobjörk and R. Österbacka, "Paper electronics," *Adv. Mater.*, vol. 23, no. 17, pp. 1935–1961, May 2011. DOI: 10.1002/adma.201004692
[34] Y. Zhang et al., "Flexible electronics based on micro/nanostructured paper," *Adv. Mater.*, vol. 30, no. 51, Dec. 2018, Art. no. 1801588, doi: 10.1002/adma.201801588.
[35] D. McManus et al., "Water-based and biocompatible 2D crystal inks for all-inkjet-printed heterostructures," *Nature Nanotechnol.*, vol. 12, no. 4, pp. 343–350, Apr. 2017, doi: 10.1038/nnano.2016.281.
[36] I. Brunetti et al., "Inkjet-printed low-dimensional materials-based complementary electronic circuits on paper," *NPJ 2D Mater. Appl.*, vol. 5, no. 1, pp. 1–6, Dec. 2021, doi: 10.1038/s41699-021-00266-5.
[37] M. Z. Pakhuruddin, K. Ibrahim, and A. A. Aziz, "Properties of polyimide substrate for applications in flexible solar cells," *Optoelectron. Adv. Mat.*, vol. 7, no. 6, pp. 377–380, 2013.
[38] G. Hu et al., "Functional inks and printing of two-dimensional materials," *Chem. Soc. Rev.*, vol. 47, no. 9, pp. 3265–3300, May 2018, doi: 10.1039/c8cs00084k.
[39] Q. Huang and Y. Zhu, "Printing conductive nanomaterials for flexible and stretchable electronics: A review of materials, processes, and applications," *Adv. Mater. Technol.*, vol. 4, no. 5, May 2019, Art. no. 1800546, doi: 10.1002/admt.201800546.
[40] N. F. Mott and F. R. S. H. H. Wills Physical, "The theory of crystal rectifiers," *Roy. Soc. London A, Math. Phys. Sci.*, vol. 171, pp. 27–38, May 1939. [Online]. Available: https://royalsocietypublishing.org/
[41] D. Tobjörk, N. J. Kaihovirta, T. Mäkelä, F. S. Pettersson, and R. Österbacka, "All-printed low-voltage organic transistors," *Organic Electron.*, vol. 9, no. 6, pp. 931–935, Dec. 2008, doi: 10.1016/j.orgel.2008.06.016.
[42] C. Martínez-Domingo, S. Conti, L. Terés, H. L. Gomes, and E. Ramon, "Novel flexible inkjet-printed metal-insulator-semiconductor organic diode employing silver electrodes," *Organic Electron.*, vol. 62, pp. 335–341, Nov. 2018, doi: 10.1016/j.orgel.2018.08.011.
[43] K. Parvez et al., "Electrochemically exfoliated graphene as solution-processable, highly conductive electrodes for organic electronics," *ACS Nano*, vol. 7, no. 4, pp. 3598–3606, Apr. 2013, doi: 10.1021/nn400576v.
[44] A. M. Nardes, M. Kemerink, M. M. de Kok, E. Vinken, K. Maturova, and R. A. J. Janssen, "Conductivity, work function, and environmental stability of PEDOT: PSS thin films treated with sorbitol," *Organic Electron.*, vol. 9, no. 5, pp. 727–734, 2008, doi: 10.1016/j.orgel.2008.05.006.
[45] B. Lyu et al., "Work function engineering of electrohydrodynamic-jet-printed PEDOT: PSS electrodes for high-performance printed electronics," *ACS Appl. Mater. Interface*, vol. 12, no. 15, pp. 17799–17805, Apr. 2020, doi: 10.1021/acsami.0c02580.
[46] J. Bardeen, "Surface states and rectification at a metal semi-conductor contact," *Phys. Rev.*, vol. 71, no. 10, p. 717, May 1947.
[47] P. Srivastava, M. Shin, K.-R. Lee, H. Mizuseki, and S. Kim, "The Schottky barrier modulation at PtSi/Si interface by strain and structural deformation," *AIP Adv.*, vol. 5, no. 8, Aug. 2015, Art. no. 087109, doi: 10.1063/1.4928323.
[48] C. Kim et al., "Fermi level pinning at electrical metal contacts of monolayer molybdenum dichalcogenides," *ACS Nano*, vol. 11, no. 2, pp. 1588–1596, Feb. 2017, doi: 10.1021/acsnano.6b07159.
[49] P. Bampoulis, R. van Bremen, Q. Yao, B. Poelsema, H. J. W. Zandvliet, and K. Sotthewes, "Defect dominated charge transport and Fermi level pinning in MoS_2/metal contacts," *ACS Appl. Mater. Interface*, vol. 9, no. 22, pp. 19278–19286, Jun. 2017, doi: 10.1021/acsami.7b02739.
[50] Y. Liu et al., "Approaching the Schottky–Mott limit in van der Waals metal-semiconductor junctions," *Nature*, vol. 557, no. 7707, pp. 696–700, May 2018, doi: 10.1038/s41586-018-0129-8.
[51] Y. H. Chen et al., "Oxidized-monolayer tunneling barrier for strong Fermi-level depinning in layered InSe transistors," *NPJ 2D Mater. Appl.*, vol. 3, no. 1, pp. 1–7, Dec. 2019, doi: 10.1038/s41699-019-0133-3.
[52] F. J. Himpsel, G. Hollinger, and R. A. Pollak, "Determination of the Fermi-level pinning position at Si(111)surfaces," *Phys. Rev. B, Condens. Matter*, vol. 28, p. 15, Dec. 1983.
[53] A. Dimoulas, P. Tsipas, A. Sotiropoulos, and E. K. Evangelou, "Fermi-level pinning and charge neutrality level in germanium," *Appl. Phys. Lett.*, vol. 89, no. 25, Dec. 2006, Art. no. 252110, doi: 10.1063/1.2410241.
[54] K. Sotthewes et al., "Universal Fermi-level pinning in transition-metal dichalcogenides," *J. Phys. Chem. C*, vol. 123, no. 9, pp. 5411–5420, Mar. 2019, doi: 10.1021/acs.jpcc.8b10971.
[55] B. G. Cook, W. R. French, and K. Varga, "Electron transport properties of carbon nanotube–graphene contacts," *Appl. Phys. Lett.*, vol. 101, no. 15, Oct. 2012, Art. no. 153501, doi: 10.1063/1.4756693.
[56] N. Izard et al., "Semiconductor-enriched single wall carbon nanotube networks applied to field effect transistors," *Appl. Phys. Lett.*, vol. 92, no. 24, Jun. 2008, Art. no. 243112, doi: 10.1063/1.2939560.
[57] G. J. Brady, A. J. Way, N. S. Safron, H. T. Evensen, P. Gopalan, and M. S. Arnold, "Quasi-ballistic carbon nanotube array transistors with current density exceeding Si and GaAs," *Sci. Adv.*, vol. 2, no. 9, Sep. 2016, doi: 10.1126/sciadv.1601240.
[58] M. Brohmann et al., "Temperature-dependent charge transport in polymer-sorted semiconducting carbon nanotube networks with different diameter distributions," *J. Phys. Chem. C*, vol. 122, no. 34, pp. 19886–19896, Aug. 2018, doi: 10.1021/acs.jpcc.8b04302.
[59] Y. Zhou, L. Hu, and G. Grüner, "A method of printing carbon nanotube thin films," *Appl. Phys. Lett.*, vol. 88, no. 12, Mar. 2006, Art. no. 123109, doi: 10.1063/1.2187945.
[60] B. Li et al., "Printing highly controlled suspended carbon nanotube network on micro-patterned superhydrophobic flexible surface," *Sci. Rep.*, vol. 5, no. 1, pp. 1–9, Oct. 2015, doi: 10.1038/srep15908.
[61] X. Huang et al., "Highly flexible and conductive printed graphene for wireless wearable communications applications," *Sci. Rep.*, vol. 5, no. 1, pp. 1–8, Dec. 2015, doi: 10.1038/srep18298.
[62] E. B. Secor, B. Y. Ahn, T. Z. Gao, J. A. Lewis, and M. C. Hersam, "Rapid and versatile photonic annealing of graphene inks for flexible printed electronics," *Adv. Mater.*, vol. 27, no. 42, pp. 6683–6688, Nov. 2015, doi: 10.1002/adma.201502866.
[63] P. He et al., "Screen-printing of a highly conductive graphene ink for flexible printed electronics," *ACS Appl. Mater. Interface*, vol. 11, no. 35, pp. 32225–32234, Sep. 2019, doi: 10.1021/acsami.9b04589.
[64] C. Wang et al., "Extremely bendable, high-performance integrated circuits using semiconducting carbon nanotube networks for digital, analog, and radio-frequency applications," *Nano Lett.*, vol. 12, no. 3, pp. 1527–1533, Mar. 2012, doi: 10.1021/nl2043375.
[65] J. Zhang, Y. Li, B. Zhang, H. Wang, Q. Xin, and A. Song, "Flexible indium–gallium–zinc–oxide Schottky diode operating beyond 2.45 GHz," *Nature Commun.*, vol. 6, no. 1, Jul. 2015, doi: 10.1038/ncomms8561.
[66] X. Zhang et al., "Solution-processed TiO_2-based Schottky diodes with a large barrier height," *IEEE Electron Device Lett.*, vol. 40, no. 9, pp. 1378–1381, Sep. 2019, doi: 10.1109/LED.2019.2928007.
[67] N. Sani et al., "All-printed diode operating at 1.6 GHz," *Proc. Nat. Acad. Sci. USA*, vol. 111, no. 33, pp. 11943–11948, Aug. 2014, doi: 10.1073/pnas.1401676111.
[68] F. Costa, S. Genovesi, M. Borgese, A. Michel, F. A. Dicandia, and G. Manara, "A review of RFID sensors, the new frontier of Internet of Things," *Sensors*, vol. 21, no. 9, p. 3138, Apr. 2021, doi: 10.3390/s21093138.
[69] K. Huang et al., "Rapid laser annealing of silver electrodes for printing organic thin-film transistors on plastic substrates," *IEEE Trans. Electron Devices*, vol. 66, no. 6, pp. 2729–2734, Jun. 2019, doi: 10.1109/TED.2019.2911310.

Open Access funding provided by 'Università di Pisa' within the CRUI CARE Agreement